Condition Assessment of Low-Speed Slew Bearings in Offshore Applications Using Acoustic Emission Monitoring

Scheeren, B.; Pahlavan, Lotfollah

DOI
10.1007/978-3-031-07322-9_90

Publication date
2022

Document Version
Final published version

Published in
European Workshop on Structural Health Monitoring

Citation (APA)
Scheeren, B., & Pahlavan, L. (2022). Condition Assessment of Low-Speed Slew Bearings in Offshore Applications Using Acoustic Emission Monitoring. In P. Rizzo, & A. Milazzo (Eds.), *European Workshop on Structural Health Monitoring: EWSHM 2022 - Volume 3* (pp. 892-901). (Lecture Notes in Civil Engineering; Vol. 270 LNCE). Springer. https://doi.org/10.1007/978-3-031-07322-9_90

Condition Assessment of Low-Speed Slew Bearings in Offshore Applications Using Acoustic Emission Monitoring

Bart Scheeren(✉) and Lotfollah Pahlavan

Faculty of Mechanical, Maritime, and Materials Engineering,
Delft University of Technology, Mekelweg 2, Delft, The Netherlands
b.scheeren@tudelft.nl

Abstract. This study presents an approach for the detection of evolving degradation in large-scale low-speed roller bearings by clustering of Acoustic Emission (AE) events, and its application to experimental degradation data. To acquire the latter, a purpose-built linear bearing, representative of a segment of a turret bearing, has been instrumented with multiple piezoelectric AE transducers in the frequency range between 40–580 kHz. Clustering based on cross-correlation has identified a number of significant clusters that are linked to the observed damage. The results suggest that condition monitoring based on AE waveform similarity clustering is suitable for detection and identification of degradation in a large-scale roller bearing.

Keywords: Acoustic emission · Condition monitoring · Roller bearing · Clustering · Offshore

1 Introduction

Permanently moored vessels in deep-sea waters, e.g. floating production storage and offloading (FPSO) units, rely heavily on large-scale roller bearings to mitigate the effects of wind and waves on heading and station-keeping. Due to the nature of those conditions, these bearings typically operate at very low speeds, while being subjected to high loads, thus risking improper lubrication redistribution, and the subsequent development of degradation. Reliability of these bearings is of high importance, and as such current design practices for these systems conservatively over-dimension the bearing, to attempt to guarantee 20 years of in-service life. However, during their service life, no major inspection takes place, and robust and reliable non-intrusive assessment remains an unresolved challenge.

Since 1969, when Balderston introduced AE techniques into the field of bearing condition monitoring [1], research has shown it to be an effective alternative to vibration monitoring, especially in high-noise environments or low-speed applications [2–4]. The origin of acoustic emissions, being irreversible changes in the microstructure of the material, attribute it the potential to detect early stage development of subsurface cracks [5–7]. This potential, however, is not yet sufficiently utilised. A common approach in AE evaluation of bearing condition monitoring is the use of

P. Rizzo and A. Milazzo (Eds.): EWSHM 2022, LNCE 270, pp. 892–901, 2023.
https://doi.org/10.1007/978-3-031-07322-9_90

artificial damage, which negates the possibility of detecting early stage development of subsurface cracking. Studies that do deal with naturally developing degradation tend to predominantly describe small-scale bearings [7–10], and high-speed applications [11–15]. A limited number of studies have attempted to assess large-scale low-speed roller bearings without artificial damage. The few that have tend to be in-situ tests, without a clear view on the actual state of the bearing [16, 17].

In this paper, detection and identification of degradation-induced ultrasonic signals in low-speed roller bearings have been experimentally investigated. The study focusses on an experimental evaluation of naturally developing degradation in a large-scale highly-loaded low-speed roller bearing.

2 Methodology

The development of degradation in a bearing, such as the initiation of a subsurface crack, is associated with the release of elastic energy. This energy propagates through the material in the form of stress waves, which experience attenuation, dispersion, reflection, and transmission, and may ultimately be detected at a location suitable for instrumentation, if they remain of sufficient energy to exceed the ultrasonic background.

2.1 Experimental Set-Up

To simulate passive ultrasonic signal generation and propagation in a large scale bearing, a test set-up that is representative of a slew or turret bearing has been designed and fabricated [18]. Figure 1 depicts this set-up. It consists of a double linear bearing, which, under vertical load applied through the support rings (component *A* in the cross-section), allows for cyclic horizontal movement of the nose ring (component *B* in the cross-section).

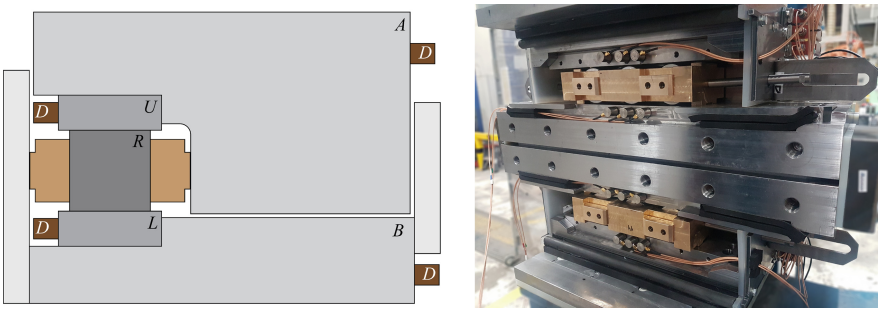

Fig. 1. Schematic overview of the top chamber of the test set-up (left), and picture of test set-up (right). Labels in the cross-section indicate the roller (*R*), nose raceway (*L*), support raceway (*U*), nose substructure (*B*), support substructure (*A*), and sensors (*D*). Note the arrangement in the picture contains a three roller configuration with tin-bronze cages, whereas the paper describes a two roller configuration with POM cages.

The raceways, rollers, and cages are all modular components. The described experiment uses; raceways with a thickness of 32.5 mm made out of Hardox 600, rollers with a diameter of 75 mm made out of 100Cr6 through hardened bearing steel, and a cage suitable for two rollers made out of polyoxymethylene (POM).

The raceways used in this experiment had already been used in an earlier natural degradation test with a 69 mm roller. In this prior test, significant wear had been developed which includes increased surface roughness, grooving, and slight pitting [18].

Instrumentation. The ultrasonic signals generated by the degradation mechanisms have been recorded in the frequency range of 40–580 kHz. To achieve this, the set-up has been instrumented on eight locations with three types of commercial piezoelectric AE transducers.

The set-up is comprised of two separate parts; the upper chamber, and the lower chamber. Due to the isolation in the middle of the nose ring, these may be considered acoustically independent from each other. Within the sphere of influence of each chamber, the measurement locations can be identified by a combination of two binary groups. Each array is situated either on the raceway, or the substructure. And that component is part of either the nose ring, or the support ring.

Finally, each location represents an array of three sensors, each of which sensitive to a specific part of the considered frequency range. The low-frequencies are covered by a 60 kHz resonant R6α, the mid-frequencies by a 150 kHz resonant R15α, and the high-frequencies by a broadband WSα – all manufactured by Physical Acoustics Corporation. Each sensor was amplified by an external AEP5H pre-amplifier set to a gain of 40 dB, before being connected to a 24 channel AMSY-6 acoustic emission measurement system fitted with ASIP-2/A signal processing cards – both manufactured by Vallen Systeme. Digital band-pass filters are applied for each sensor type individually to separate low-, mid- and high-frequency content. For the low-frequency measurement channels, a band-pass from 40–100 kHz is set, for the mid-frequency, 95–180 kHz, and for the high-frequency, 180–580 kHz.

Whenever a 50 dB threshold was crossed, a transient recording of 812 μs was sampled at 5 MHz. This transient recording contains a 200 μs pre-trigger recording to capture the onset of the detected signal prior to crossing of the threshold.

2.2 Experimental Procedures

An arrangement of two rollers is subjected to a vertical load of 1305 kN, while a horizontal stroke of 70 mm is cycled through every 12 s for a linear speed of about 0.012 m/s. The test is continued for 100,000 cycles (approximately 333 h). During the test, the set-up is lubricated daily with Mobilux EP2 heavy duty grease. To compensate for slipping, the rollers and cages in the set-up are repositioned whenever they have travelled more than 45 mm from the centred position. Additionally three inspections were executed.

2.3 Data Processing

Prior to processing, the data is filtered for the signal-to-noise ratio (SNR) and test machine operation. The implemented SNR filter divides each recorded waveform into a pre-trigger window and a post-trigger window. The peak amplitudes of these two windows are compared, and if the signal exceeds the noise by at least 10 dB it is retained. Test machine operations are used to define a start-stop filter. Initial data processing has shown that acceleration of the nose ring is associated with the release of AE signals. These are removed by detecting when the testing machine is stationary, and rejecting all hits in a tolerance zone of 2.5% of the nominal stroke around that stationary point.

Clustering. The shape of a waveform observed at a certain location is uniquely defined by the mechanism of emission and the propagation path. This can be used to identify mechanisms that consistently emit waveforms, of which cracking is the most notable example. Implementation is based on cross-correlation, which is defined as

$$(f \bigstar g)(\tau) \equiv \int_{-\infty}^{\infty} \overline{f}(t-\tau) g(t) dt, \tag{1}$$

for two arbitrary signals f and g in the time domain. The cross correlation is determined for a particular time shift τ, and when a range of time shifts are considered, the absolute maximum indicates the highest similarity between the two waveforms. This similarity is obtained through

$$\varsigma_{f,g} = \max\left(\left|\frac{(g \bigstar f)(\tau)}{\sqrt{(g \bigstar g)(0)(f \bigstar f)(0)}}\right|\right). \tag{2}$$

In this equation the denominator of the fraction represents a normalisation of the cross-correlation. As such the resulting value is contained within the closed interval [0, 1], where the extremes represent the cases of identical or polar opposite waves ($\varsigma_{f,g} = 1$), or no similarity at all ($\varsigma_{f,g} = 0$).

Knowing the similarity, signals may be clustered. For this procedure, dissimilarity is used. The dissimilarity is defined as

$$\delta_{f,g} = 1 - \varsigma_{f,g}. \tag{3}$$

A common approach to identify structure in waveform dissimilarity is agglomerative hierarchical clustering [19, 20]. A downside of this approach is the requirement to have all data available at the beginning, preventing on-line implementation for condition monitoring. Alternative sequential algorithms for clustering have been proposed, such as one by Pomponi and Vinogradov [21] for clustering AE power spectra. These procedures could in essence be reduced to comparing each newly acquired signal, to the already existing clusters, and assigning it to either one of those clusters or declare it a new cluster.

A similar algorithm has been implemented. By order of detection, each AE signal is compared to the existing clusters (assuming there are existing clusters, if not, it is assigned non-clustered). In case the cluster dissimilarity is below the set limit of 0.3, the signal will be added to that cluster. In case no cluster exists which meets this criterion, the signal is compared to the last 250 non-clustered signals. In case the dissimilarity with any of these signals is less than 0.3, a new cluster is generated. Otherwise, the signal is added to the collection of the last 250 non-clustered signals.

To speed up the processing, each new signal is not compared to all waveforms that already compose a cluster. Instead a sample of nine waveforms is selected to represent the cluster. These nine signals are randomly selected in groups of three from; the original ten signals that form the cluster, the last ten signals that have been added to the cluster, and any other wave that is a part of the cluster.

Comparing multiple signals, and thus multiple dissimilarities to each other is required when clusters are formed and start to grow. To compare a new signal g to an existing cluster c that is composed of N signals f, a mean dissimilarity is determined by

$$\delta_g^c = \frac{\sum_{f=1}^{N} w_f \delta_{f,g}}{\sum_{f=1}^{N} w_f}, \text{wherein } f \in c. \tag{4}$$

Here w_f indicates a weight factor, which has been implemented into the sequential clustering algorithm to increase the importance of the latest waveforms that have been added to the cluster. The weight factor is set to give the latest three signals double weight compared to the first three signals. The arbitrary three signals are assigned a neutral weight. The total weight has been set to be equal to the amount of signals.

3 Results

To evaluate the clustering methodology, an experiment was performed wherein further damage was induced on already worn raceways. A total of 92,915 cycles were performed at a load of 1305 kN. During the test two inspections have been performed in addition to the final inspection at the end of the experiment. Over the course of the test some small cracks formed in the raceways on the edges of the wear patterns that originated from prior testing with a smaller roller with a width of 69 mm [18].

An extensive amount of ultrasonic signals has been recorded during the experiment. For the sake of brevity, the results are solely discussed for the top chamber. The ultrasonic activity is shown in Fig. 2 as the hit-rate per cycle. Note that a cycle of the test machine constitutes a forward and a backward stroke.

The graphs show that the support side of the set-up generally has a higher ultrasonic activity than the nose side. The activity on the raceways for the most part closely matches the activity on the substructure, with the biggest differences observed for the low-frequency channels. These generally display a higher activity on the substructure

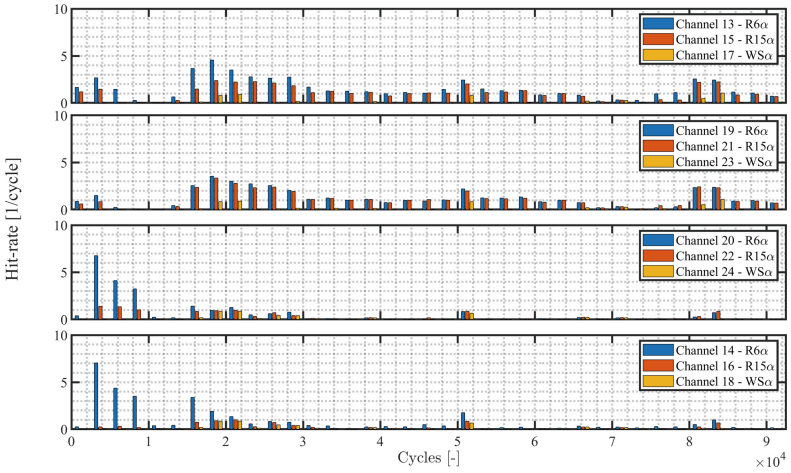

Fig. 2. Ultrasonic activity in top chamber, averaged per 2,500 cycles, separated in graphs per location: support substructure (top), support raceway (upper-middle), nose raceway (lower-middle), and nose substructure (bottom).

in comparison to the raceway, which is likely due to low-frequency sources outside of the set-up.

Considering the geometry of the set-up, and earlier work on the transmission of elastic stress waves in bearings [22], AE associated with development of significant degradation is regarded detectable on both raceways. Development of degradation is expected around 15,000–30,000 cycles, at 50,000 cycles, and at 80,000–85,000 cycles. Taking the inspections into account, at 28,099 cycles no significant visual change in the wear condition was observed relative to the start of the experiment, while at 60,463 cycles small cracks were observed in the raceways. This might indicates the small peak at 50,000 cycles originates from crack growth. Alternatively increased activity before these observations could indicate crack initiation. During the final inspection at 92,915 cycles no significant change is observed visually.

To further evaluate the observations regarding the development of the small cracks, the data has been clustered to identify similar source mechanisms, which can indicate similar degradation types. For each measurement channel the largest 50 clusters have been evaluated. Common trends have been identified, leading to the two structures of clusters that are presented in Fig. 3 and Fig. 4. Both of these structures span a range of approximately 2,000 cycles, and they mark the respective end of the increased activity just before 30,000 cycles and the peak observed at 50,000 cycles.

The structure in Fig. 3 is composed of low- and mid-frequency signals. In the evaluated clusters, no matching high-frequency trend was observed. Note that only the 50 largest clusters have been evaluated, and thus a matching structure may be identified if a larger sample of clusters is evaluated. The structure shows a trend that is first increasing in amplitude, and then decreasing, before disappearing. The end of the structure occurs right when the test machine stops before the first inspection at 28,099 cycles. The amplitudes in the structure display a highly consistent behaviour, indicating

consistency in the energy that is emitted by the emission mechanism. The ratios between the amplitudes recorded on the different measurement channels suggest the emission mechanism is originating from the nose side of the set-up. The high amplitudes on measurement channel 14 (substructure) compared to channel 20 (raceway) and the near equal amplitudes on channels 16 (substructure) and 22 (raceway) indicate the source is likely not located on the raceway. As such, the cluster is probably not related to development of degradation.

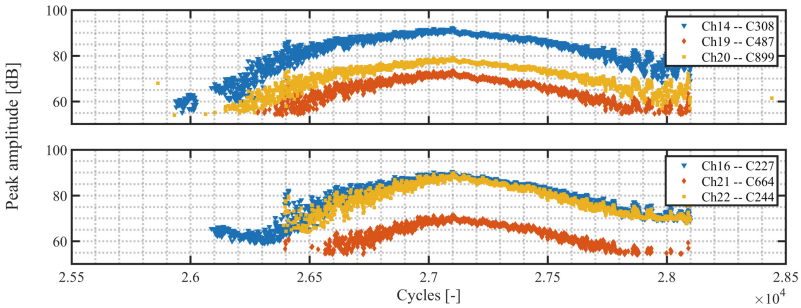

Fig. 3. Structure of clusters at 26,000–28,000 cycles consisting of selected clusters from low- (top) and mid-frequency (bottom) measurement channels.

The structure in Fig. 4 is composed of all considered frequency ranges. It has been identified on all measurement channels, except for the low-frequency substructure channels. Notable are the clusters identified on channel 15 (cluster 612 & cluster 618) which have been identified as different clusters by the algorithm, but have been observed to compose a shared trend. Similarly notable is the cluster identified on channel 17 (cluster 297), which has only been identified for the first one-third of the structure. To continue this trend, smaller clusters have probably been identified by the algorithm, which were not discovered in the evaluation of the 50 largest clusters. Both channels 15 and 17 are located on the support substructure, which seems to be the location furthest from the source. This might indicate that clustering becomes more susceptible to small variations in the signals as the propagation distance increases.

The ratios between amplitudes of the different measurement channels indicate the clusters originate on the nose raceway. This evaluation is slightly complicated by the occurrence of saturation of the measurement system for some mid- and high-frequency channels, however, the high-frequency graph suggests a difference in amplitude of 20 dB for signals recorded on the nose or support side of the set-up, indicating the nose side as the origin of the emission. Additionally the difference of 5 dB between the raceway and substructure channels indicates the signals originate from the raceway. The source location and time of emission, in combination with the observations from visual inspection, strongly suggest this cluster is related to crack growth.

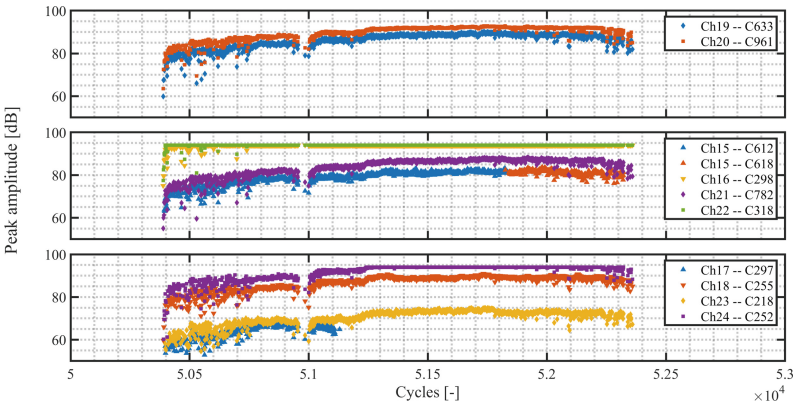

Fig. 4. Structure of clusters at 50,000–52,500 cycles consisting of selected clusters from low- (top), mid-(middle), and high-frequency (bottom) measurement channels.

4 Conclusions

Experiments have been performed to study the potential of AE techniques to detect and classify the inception and development of degradation in a large-scale highly-loaded low-speed roller bearing. Over the course of 92,915 cycles, severe wear was further developed and small cracks were formed in the raceways. Several inspections describe the progression of this failure. Hit-rate-based analysis of the AE activity seemed to match the increased degradation observed during inspections. Clustering identified several larger structures of correlated waveforms among different measurement channels, of which one is suggestive of a highly similar emission mechanism in the nose raceway of the top chamber. Also considering the inspections and ultrasonic activity over the whole test, this similarity is likely to be indicative of a crack growth. The study shows good potential for applying cross-correlation based clustering for AE condition monitoring of highly-loaded low-speed roller bearings.

Acknowledgements. This research has been conducted within the framework of HiTeAM Joint Industry Programme. The project partners, i.e. Total, SBM Offshore, Sofec, Heerema Marine Contractors, Huisman Equipment, Allseas Engineering, and Bluewater Energy Services are acknowledged for their contribution. Huisman Equipment, Bluewater Energy Services and Sofec are additionally acknowledged for providing extensive support in the design and production of the test bearing and in the execution of the experiment.

This project has been made possible by a financial contribution of TKI Maritime.

References

1. Balderston, H.L.: The detection of incipient failure in bearings. Mater. Eval. **27**, 121–128 (1969)
2. Tandon, N., Nakra, B.C.: Comparison of vibration and acoustic measurement techniques for the condition monitoring of rolling element bearings. Tribol. Int. **25**, 205–212 (1992). https://doi.org/10.1016/0301-679X(92)90050-W

3. Hawman, M.W., Galinaitis, W.S.: Acoustic emission monitoring of rolling element bearings. Ultrason. Symp. Proc. **2**, 885–889 (1988). https://doi.org/10.1109/ultsym.1988.49503
4. Al-Ghamd, A.M., Mba, D.: A comparative experimental study on the use of acoustic emission and vibration analysis for bearing defect identification and estimation of defect size. Mech. Syst. Signal Process. **20**, 1537–1571 (2006). https://doi.org/10.1016/j.ymssp.2004.10.013
5. Elforjani, M., Mba, D.: Monitoring the onset and propagation of natural degradation process in a slow speed rolling element bearing with acoustic emission. J. Vib. Acoust. Trans. ASME. **130**, 1–14 (2008). https://doi.org/10.1115/1.2948413
6. Fuentes, R., Dwyer-Joyce, R.S., Marshall, M.B., Wheals, J., Cross, E.J.: Detection of subsurface damage in wind turbine bearings using acoustic emissions and probabilistic modelling. Renew. Energy. **147**, 776–797 (2020). https://doi.org/10.1016/J.RENENE.2019.08.019
7. Cornel, D., Gutiérrez Guzmán, F., Jacobs, G., Neumann, S.: Condition monitoring of roller bearings using acoustic emission. Wind Energy Sci. **6**, 367–376 (2021). https://doi.org/10.5194/WES-6-367-2021
8. Miettinen, J., Pataniitty, P.: Acoustic emission in monitoring extremely slowly rotating rolling bearing. In: Proceedings of COMADEM 1999, 6–9 July 1999, pp. 289–297. Coxmoore Publishing Company, Sunderland (1999)
9. Elforjani, M., Mba, D.: Observations and location of acoustic emissions for a naturally degrading rolling element thrust bearing. J. Fail. Anal. Prev. **8**, 370–385 (2008). https://doi.org/10.1007/s11668-008-9141-x
10. Sako, T., Yoshie, O.: Diagnostic method of low speed rolling element bearing using AE envelope waveform. In: IEEE Region 10 Annual International Conference Proceedings/TENCON, pp. 724–729 (2010). https://doi.org/10.1109/TENCON.2010.5686610
11. Yoshioka, T., Fujiwara, T.: A new acoustic emission source locating system for the study of rolling contact fatigue. Wear **81**, 183–186 (1982). https://doi.org/10.1016/0043-1648(82)90314-3
12. Eftekharnejad, B., Carrasco, M.R., Charnley, B., Mba, D.: The application of spectral kurtosis on acoustic emission and vibrations from a defective bearing. Mech. Syst. Signal Process. **25**, 266–284 (2011). https://doi.org/10.1016/j.ymssp.2010.06.010
13. Rahman, Z., Ohba, H., Yoshioka, T., Yamamoto, T.: Incipient damage detection and its propagation monitoring of rolling contact fatigue by acoustic emission. Tribol. Int. **42**, 807–815 (2009). https://doi.org/10.1016/j.triboint.2008.10.014
14. Williams, T., Ribadeneira, X., Billington, S., Kurfess, T.: Rolling element bearing diagnostics in run-to-failure lifetime testing. Mech. Syst. Signal Process. **15**, 979–993 (2001). https://doi.org/10.1006/mssp.2001.1418
15. Yoshioka, T., Korenaga, A., Mano, H., Yamamoto, T.: Diagnosis of rolling bearing by measuring time interval of ae generation. J. Tribol. **121**, 468–472 (1999). https://doi.org/10.1115/1.2834091
16. Rogers, L.M.: The application of vibration signature analysis and acoustic emission source location to on-line condition monitoring of anti-friction bearings. Tribol. Int. **12**, 51–58 (1979). https://doi.org/10.1016/0301-679X(79)90001-X
17. Mba, D., Bannister, R.H., Findlay, G.E.: Condition monitoring of low-speed rotating machinery using stress waves part 1. Proc. Inst. Mech. Eng. Part E J. Process Mech. Eng. **213**, 153–170 (1999). https://doi.org/10.1243/0954408991529906
18. Scheeren, B., Huijer, A., Riccioli, F., Thakoerdajal, N., Pahlavan, L.: HiTeAM - report phase 2 (2021)

19. Huijer, A., Kassapoglou, C., Pahlavan, L.: Acoustic emission monitoring of carbon fibre reinforced composites with embedded sensors for in-situ damage identification. Sensors. **21**, 6926 (2021). https://doi.org/10.3390/s21206926
20. Van Steen, C., Pahlavan, L., Wevers, M., Verstrynge, E.: Localisation and characterisation of corrosion damage in reinforced concrete by means of acoustic emission and X-ray computed tomography. Constr. Build. Mater. **197**, 21–29 (2019). https://doi.org/10.1016/J.CONBUILDMAT.2018.11.159
21. Pomponi, E., Vinogradov, A.: A real-time approach to acoustic emission clustering. Mech. Syst. Signal Process. **40**, 791–804 (2013). https://doi.org/10.1016/J.YMSSP.2013.03.017
22. Scheeren, B., Kaminski, M.L., Pahlavan, L.: Evaluation of ultrasonic stress wave transmission in cylindrical roller bearings for acoustic emission condition monitoring. Sensors **22**, 1500 (2022). https://doi.org/10.3390/S22041500